Specific features in the band structure and linear and nonlinear optical susceptibilities of $La_2CaB_{10}O_{19}$ crystals

Ali Hussain Reshak,[1] S. Auluck,[2] and I. V. Kityk[3]
[1]*Institute of Physical Biology-South Bohemia University, Institute of System Biology and Ecology-Academy of Sciences, Nove Hrady 37333, Czech Republic*
[2]*Physics Department, Indian Institute of Technology, Roorkee (Uttaranchal) 247667, India*
[3]*Institute of Physics, J. Dlugosz University of Czestochowa, Al. Aermii Krajowj 13/15, Czestochowa, Poland*
(Received 7 February 2007; revised manuscript received 17 April 2007; published 21 June 2007)

The electronic and optical properties have been calculated for monoclinic $La_2CaB_{10}O_{19}$ (LCB) crystal using the state-of-the-art full potential linear augmented plane wave method. We present results for the band structure, density of states, birefringence, imaginary and real parts of the frequency dependent linear and nonlinear optical response. We have found that LCB is a semiconductor with an indirect energy band gap of about 4.45 eV. A simple scissor operator is applied to adjust the band energy gap from the calculations to match the experimental value (5.4 eV). The calculated birefringence of the LCB crystal has positive sign in agreement with the experimental data. Calculations are reported for the frequency-dependent complex second-order nonlinear optical susceptibilities $\chi^{(2)}_{abc}(\omega)$ up to 6 eV and for zero-frequency limit $\chi^2(0)$. LCB exhibits second harmonic generation efficiency about two times larger than KDP crystal (KH_2PO_4).

DOI: 10.1103/PhysRevB.75.245120 PACS number(s): 71.15.Ap

I. INTRODUCTION

Many borate-crystals show promising nonlinear optical properties (NLO) compared to the well known inorganic compounds.[1] These borates (in form of single crystals) find numerous applications in laser and NLO applications. These crystals play an important role in ultraviolet (UV) applications due to their relatively high UV transparency, good NLO efficiency and high damage threshold for laser radiation. These crystals allow efficient generation of radiation in UV and visible region due to possibility of higher optical harmonics generation of external laser sources or self-frequency doubling (SFD) when they act simultaneously as a laser and second-order NLO material. In the recent years, visible and UV lasers have been in demand for many industrial, medical and entertainment applications. Frequency conversion of a solid-state laser such as a Nd:YAG laser by means of NLO crystal is the most promising way to obtain such coherent light. For efficient laser frequency conversion, NLO crystals are very important.[2] One of the new promising borate crystals showing NLO properties is lanthanum calcium borate $La_2CaB_{10}O_{19}$ (LCB). LCB is a new NLO crystal discovered by Wu's group.[2–5] The LCB semiconductor crystal, which crystallizes in the monoclinic structure, has received much attention in recent years.[2–6]

The dynamical properties of LCB crystals are described by many workers.[2–6] There is interest in their hardness.[3] Yet up to now there is no comprehensive work related to the electronic structure, frequency dependent linear optical properties, birefringence, and frequency dependent nonlinear optical (NLO) properties of LCB, although their potential NLO applications have been emphasized. A comprehensive understanding of the origin of the optical nonlinearity of these materials and the origin of the high $\chi^{(2)}(\omega)$ are crucial for their further applications. One of restraining factor to find promising methods for further improvement of their quality is an absence of reliable energy band structure. This may be related to the relatively complicated structure of these crystals. In the current work, we will present a state-of-the-art study of the optical susceptibility spectral features using the band energy structure obtained from a full potential calculation.

To the best of our knowledge there are no full potential theoretical calculations for the band structure, linear optical properties, and nonlinear properties for LCB. Moreover, the existed experimental data is poor. Earlier we had studied the electronic properties of LCB using the first-principle self-consistent, tight-binding (TB) linear muffin tin orbital (LMTO) based on the muffin-tin approximation.[6] A natural extension would be to study their linear and nonlinear optical properties (susceptibilities). As these require very accurate wave-functions we decided to use a full potential method. The muffin-tin approximation (MTA) works reasonably well in highly coordinated systems, such as face-centered cubic (fcc) metals. For covalently bonded solids or layered structures (as in our case) the MTA is a poor approximation and leads to discrepancies with experiments (we mentioned some discrepancies in our pervious work[7]). The more general treatment of the potential, such as provided by a full potential (FP) method has none of the drawbacks of the atomic sphere approximation (ASA) and MTA based methods. In full potential methods the potential and charge density are expanded into lattice harmonics inside each atomic sphere and as a Fourier series in the interstitial region. We therefore thought it worthwhile to perform *ab initio* calculations using a full potential method which has proven to be one of the most accurate methods[8,9] for the computation of the electronic structure of solids within a framework of density functional theory (DFT) approach. Our calculations will demonstrate the effect of using a full-potential on the band structure and density of states. Our aim in this paper is to understand the origin of the high $\chi^{(2)}_{abc}(\omega)$ susceptibilities. To verify the performed theoretical calculations we compare the calculated birefringence with the available experimental data.

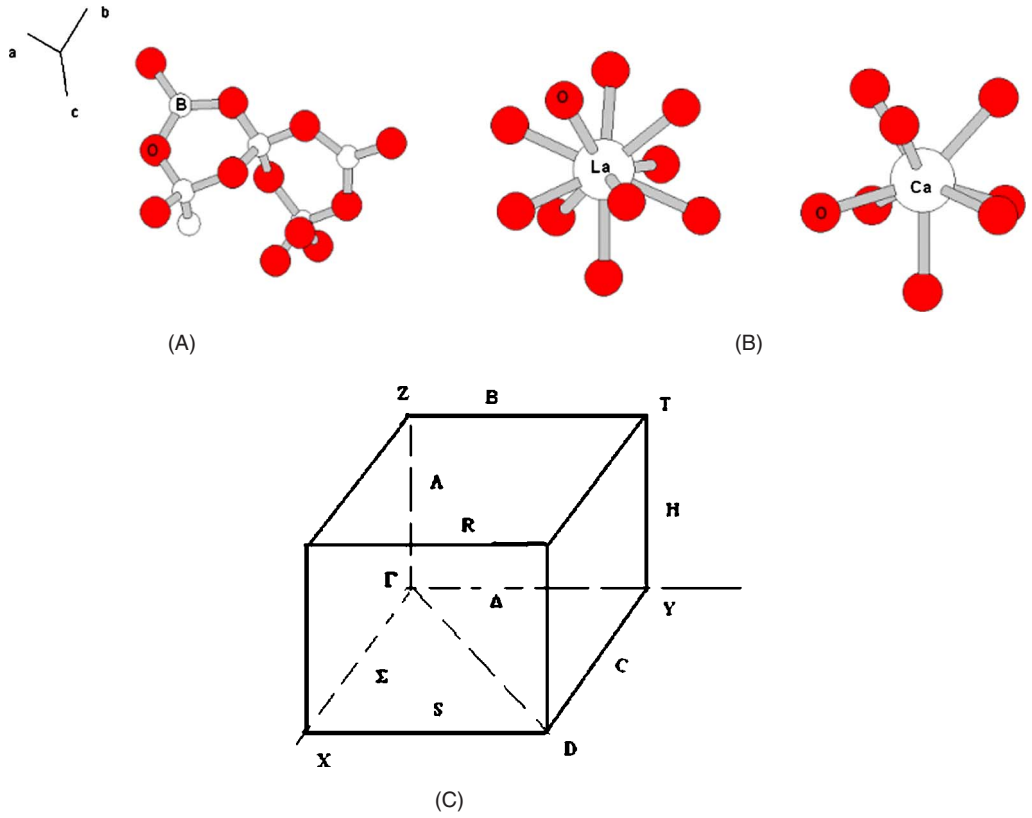

FIG. 1. (Color online) (A) The B_5O_{12} group. (B) Oxygen coordination to the La and Ca atoms. (C) Brillouin zone of the $C2$ group.

In Sec. II we give details of our calculations. The theoretically calculated band structure, densities of states, the linear and nonlinear optical susceptibilities, and birefringence are presented and discussed in Sec. III. In Sec. IV we summarize our conclusions.

II. DETAILS OF CALCULATIONS

$La_2CaB_{10}O_{19}$ is a biaxial single crystal which belongs to the monoclinic system with space group $C2$ with two formula units per cell.[2] The lattice parameters of LCB crystal are $a=11.043$ Å, $b=6.563$ Å, $c=9.129$ Å, $\alpha=\gamma=90°$, and $\beta=91.47°$. The LCB crystal is a member of the newly synthesized NLO borate crystals RCB ($R_2CaB_{10}O_{19}$) family, where R represents rare-earth elements.[10] LCB is absolutely insensitive to moisture, and has a hardness of 6.5 Mohs, allowing easy cutting and optical polishing.[2] The crystal structure contains B_5O_{12} double-ring pentaborate groups, which are linked together forming infinite two-dimensional double layer. The layer is situated almost perpendicularly to the c axis of the crystal. The La atoms are located in layers, while Ca atoms are located between two layers (Fig. 1).

In our calculations we use the state-of-the-art full potential linear augmented plane wave (FPLAPW) method in a scalar relativistic version as embodied in the WIEN2K code.[11] This is an implementation of the density-functional theory (DFT) with different possible approximations for the exchange-correlation (XC) potential. XC is treated within the local density approximation[12] (LDA) and scalar relativistic equations are used to obtain self-consistency. The Kohn-Sham equations are solved using a basis of linear APW's.

In order to achieve energy eigenvalues convergence, the wave functions in the interstitial region were expanded in plane waves with a cutoff $K_{max}=7/R_{MT}$, where R_{MT} denotes the smallest atomic sphere radius and K_{max} gives the magnitude of the largest K vector in the plane wave expansion. The R_{MT} are taken to be 2.0, 1.6, 1.3, and 1.1 atomic units (a.u.) for La, Ca, O, and B respectively. The valence wave functions in side the spheres are expanded up to $l_{max}=10$ while the charge density was Fourier expanded up to $G_{max}=14$.

Self-consistency is achieved using 170 $\vec{k}$ points in the irreducible Brillouin zone (IBZ). We calculate the frequency dependent linear optical properties using 500 $\vec{k}$ points and nonlinear optical properties using 1000 $\vec{k}$ points in the IBZ.

III. RESULTS AND DISCUSSION

A. Band structure and density of states

The band structure and total density of states (TDOS), along with La-$s/p/d/f$, Ca-s/p, B-s/p, and O-s/p partial densities of states (PDOS) for LCB crystal are shown in Fig. 2. The valence band maximum (VBM) is located at Γ while the conduction band minimum (CBM) is located at M resulting in an indirect energy gap of 4.45 eV. The calculated energy gap is smaller than the experimental gap (5.4 eV) as expected from LDA calculation.[13] The band structure and hence the density of states (DOS) can be divided into four

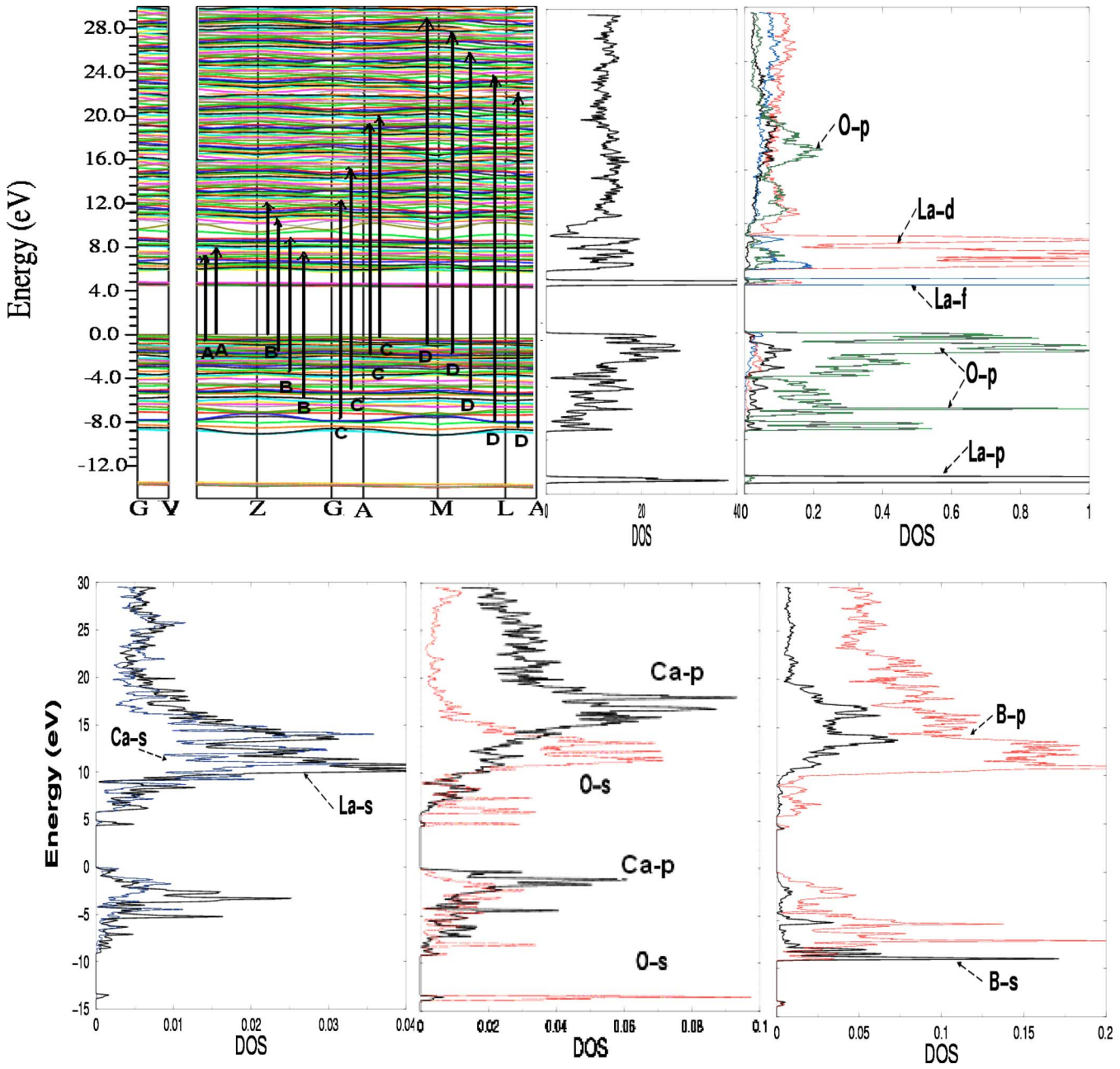

FIG. 2. (Color online) Band structure and total density of states (states /eV unit cell), along with La-$s/p/d/f$, Ca-s/p, B-s/p, and O-s/p partial densities of states. The optical transitions depicted on a generic band structure.

groups/structures. From the PDOS we are able to identify the angular momentum (l-dependent) origin of the various structures. The lowest energy group has mainly La-p state's origin. The second group between −9.0 eV and Fermi energy (E_F) has significant contributions from O-p states. The third group, the lowest conduction band (at 4.5 and 5.0 eV) is found to be La-f states, separated from the next more complex group. The band gap is governed by the location of the La-f states. We expect our calculated band gap to be smaller than the measured band gap. The conventional band gap in LDA is not easy to fix by methods other than either very primitive (scissor) or quite sophisticated (GW), for localized states such as La-f. So we can say that the position of La-f band as it comes from LDA calculations is very much off. The last group from −5.5 to 8.0 eV is due to La-d with some contribution from La-p, La-/f, and O-p states. The electronic structure of the upper valence band arises primarily from the La-d and La-p interactions. We note that most of the La-d states are concentrated in the upper conduction band, with negligible contribution to the valence band. Most of the La-p states are pushed from the conduction bands into valence bands. From the PDOS, we note a strong hybridization between La-d, La-p and La-f states below E_F. Also there is a strong hybridization between Ca-s and La-s, and Ca-p with O-s below and above E_F. Following Yamasaki *et al.*[14] we can define degree of hybridization by the ratio of La-d

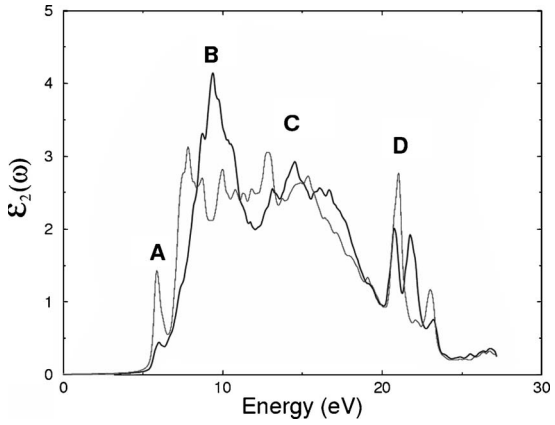

FIG. 3. Calculated $\varepsilon_2^{\perp}(\omega)$ (dark curve) and $\varepsilon_2^{\parallel}(\omega)$ (light curve).

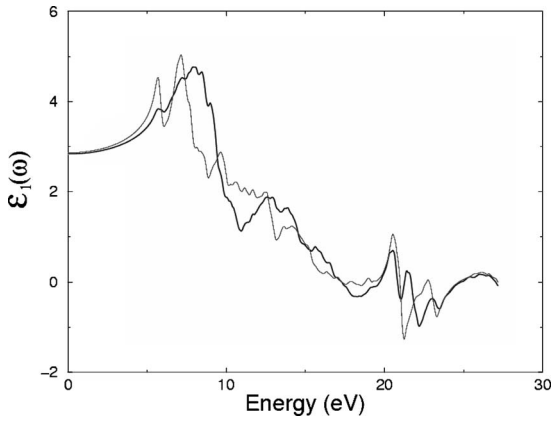

FIG. 4. Calculated $\varepsilon_1^{\perp}(\omega)$ (dark curve) and $\varepsilon_1^{\parallel}(\omega)$ (light curve).

states and La-p states within the muffin tin sphere. Based on this we can say that the hybridization between La-d and La-p, La-f states becomes weak in the conduction band.

B. Linear optical response and birefringence

Since the investigated compound has monoclinic symmetry, there are many components of the dielectric tensor. We will concentrate on the major components, corresponding to electric field $\vec{E}$ perpendicular and parallel to the c axis. These are $\varepsilon_2^{\perp}(\omega)$ and $\varepsilon_2^{\parallel}(\omega)$, respectively, the imaginary parts of the frequency dependent dielectric function. We have performed calculations of the frequency dependent dielectric function for these compounds using the expressions[15,16]

$$\varepsilon_2^{\parallel}(\omega) = \frac{12}{m\omega^2}\int_{\mathrm{BZ}} \sum \frac{|P^Z_{nn'}(k)|^2 dS_k}{\nabla \omega_{nn'}(k)},$$

$$\varepsilon_2^{\perp}(\omega) = \frac{6}{m\omega^2}\int_{\mathrm{BZ}} \sum \frac{[|P^X_{nn'}(k)|^2 + |P^Y_{nn'}(k)|^2] dS_k}{\nabla \omega_{nn'}(k)}.$$

The above expressions are written in atomic units with $e^2=1/m=2$ and $\hbar=1$, where ω is the photon energy and $P^X_{nn}(k)$ is the x component of the dipole matrix elements between initial $|nk\rangle$ and final $|n'k\rangle$ states with their eigenvalues $E_n(k)$ and $E_{n'}(k)$, respectively. Here $\omega_{nn'}(k)$ is the band energy difference $\omega_{nn'}(k)=\{E_n(k)-E_{n'}(k)\}$ and S_k is a constant energy surface $S_k=\{k;\omega_{nn'}(k)=\omega\}$.

Figure 3 shows the calculated imaginary part of the frequency dependent dielectric functions $\varepsilon_2^{\perp}(\omega)$ and $\varepsilon_2^{\parallel}(\omega)$. A considerable anisotropy is found between these components. The broadening is taken to be 0.04 eV. Our optical properties are scissors corrected[17,18] by 0.95 eV. This is the difference between the calculated and measured energy gap.

It would be worthwhile to attempt to identify the band transitions that are responsible for the spectral structures in $\varepsilon_2^{\perp}(\omega)$ and $\varepsilon_2^{\parallel}(\omega)$ using our calculated band structure. Figure 2, show the transitions which are responsible for the spectral structures in $\varepsilon_2^{\perp}(\omega)$ and $\varepsilon_2^{\parallel}(\omega)$. For simplicity we have labeled the transitions in Figs. 2 and 3, as A, B, C, and D. The transitions A are responsible for the structures in $\varepsilon_2^{\perp}(\omega)$ and $\varepsilon_2^{\parallel}(\omega)$ for energies up to 7.5 eV, transitions B for the structures in the energy range 7.5–12.5 eV, transitions C for the structures between 12.5 and 20.0 eV, and transitions D for the structures between 20.0 and 30.0 eV.

From the imaginary part of the dielectric function $\varepsilon_2^{\perp}(\omega)$ and $\varepsilon_2^{\parallel}(\omega)$ the real part $\varepsilon_1^{\perp}(\omega)$ and $\varepsilon_1^{\parallel}(\omega)$ is calculated by using Kramers-Kronig relations.[19] The results of our calculated $\varepsilon_1^{\perp}(\omega)$ and $\varepsilon_1^{\parallel}(\omega)$ are shown in Fig. 4. The calculated value of $\varepsilon_1^{\perp}(0)$ and $\varepsilon_1^{\parallel}(0)$ is about 2.9.

LCB shows considerable anisotropy which favors SHG. The birefringence is important in fulfilling phase-matching conditions. The birefringence can be calculated from the linear response functions from which the anisotropy of the index of refraction is obtained. The refractive indices for the ordinary and extraordinary rays can be calculated following the expression:[20]

$$n(\omega) = (1/\sqrt{2})[\sqrt{\varepsilon_1(\omega)^2 + \varepsilon_2(\omega)^2} + \varepsilon_1(\omega)]^{1/2}.$$

The birefringence is the difference between the extraordinary and ordinary refraction indices, $\Delta n = n_e - n_o$, where n_e is the index of refraction for an electric field oriented along the c axis and n_0 is the index of refraction for an electric field perpendicular to the c axis.

Figure 5 shows the birefringence $\Delta n(\omega)$ for the LCB. The birefringence is important only in the nonabsorbing region, which is below the energy gap. The $\Delta n(\omega)$ curve shows strong oscillations throughout the energy range. This is due to the small broadening (0.04 eV) that we have taken for calculating the frequency dependent dielectric functions. We find that the zero energy birefringence $\Delta n(0)=0.049$ in reasonable agreement with the experimental[3] value of 0.053. The birefringence of LCB is larger than that of $YCa_4O(BO_3)_3$ (YCOB).[3] In past few years YCOB crystal has generated considerable interest because it exhibits a relatively large birefringence and SHG effect.[21]

C. Nonlinear response

The complex second-order nonlinear optical susceptibility tensor $\chi^{(2)}_{abc}(-2\omega;\omega;\omega)$ can be written as the sum of three different contributions in the form[22]

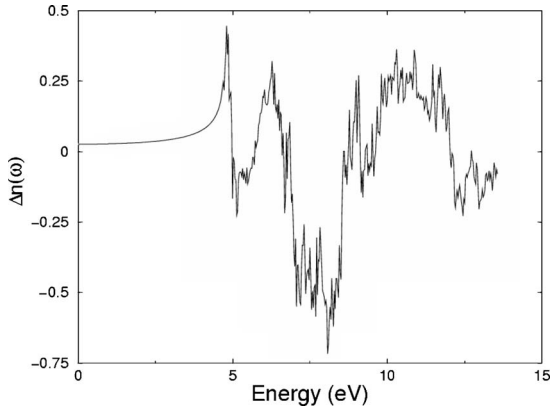

FIG. 5. Calculated $\Delta n(\omega)$.

$$\chi^{abc}_{\text{int } er}(-2\omega;\omega;\omega) = \frac{e^3}{\hbar^2\Omega}\sum_{cvn,k}\frac{r^a_{vc}\{r^b_{cn}r^c_{nv}\}}{(\omega_{nv}-\omega_{cn})}\left[\frac{2f_{vc}}{\omega_{cv}-2\omega}+\frac{f_{nc}}{\omega_{nc}-\omega}+\frac{f_{vn}}{\omega_{vn}-\omega}\right],$$

$$\chi^{abc}_{\text{int } ra}(-2\omega;\omega;\omega) = \frac{ie^3}{2\hbar^2\Omega}\sum_{cv,k} f_{vc}\left[\frac{2}{\omega_{cv}(\omega_{cv}-2\omega)}r^a_{vc}(r^b_{vc;c}+r^c_{cv;b}) + \frac{1}{\omega_{cv}(\omega_{cv}-\omega)}(r^a_{vc;c}r^b_{cv}+r^a_{vc;b}r^c_{cv}) + \frac{1}{\omega^2_{cv}}\left(\frac{1}{\omega_{cv}-\omega}-\frac{4}{\omega_{cv}-2\omega}\right)r^a_{vc}(r^b_{cv}\Delta^c_{cv}+r^c_{cv}\Delta^b_{cv}) \times\frac{1}{2\omega_{cv}(\omega_{cv}-\omega)}(r^b_{vc;a}r^c_{cv}+r^c_{vc;a}r^b_{cv})\right].$$

In which $\{r^b_{nv}r^c_{vc}\}=(1/2)(r^b_{nv}r^c_{vc}+r^c_{nv}r^b_{vc})$ is a symmetrized combination of the dipole matrix elements $r^a_{cn}=\delta_{cn}P^a_{cn}/im\omega_{cn}$, which are obtained from the momentum matrix elements P^a_{cn}. Superscripts (a,b,c) refer to the cartesian indices. The index v stands for a valence band state and c for the conduction band state and n the intermediate band, which is either in the valence or conduction band. It has been demonstrated by Aspnes[23] that transitions involving one valence band state and two conduction band states give a significant contribution to the second order tensor. Here we have ignored the virtual-hole contribution (transitions involving two valence band states and one conduction band state) because it is an order of magnitude smaller. For simplicity we call $\chi^{(2)}_{abc}(-2\omega;\omega;\omega)$ as $\chi^{(2)}_{abc}(\omega)$. Since the LCB crystal belongs to the point group $C2$ there are eight independent components of the SHG tensor, namely, the 123, 112, 211, 222, 233, 231, 332, and 312 components (1, 2, and 3 refer to the x, y, and z axes, respectively).[24] These yield $\chi^{(2)}_{123}(\omega),\ldots\ldots$, and $\chi^{(2)}_{312}(\omega)$.

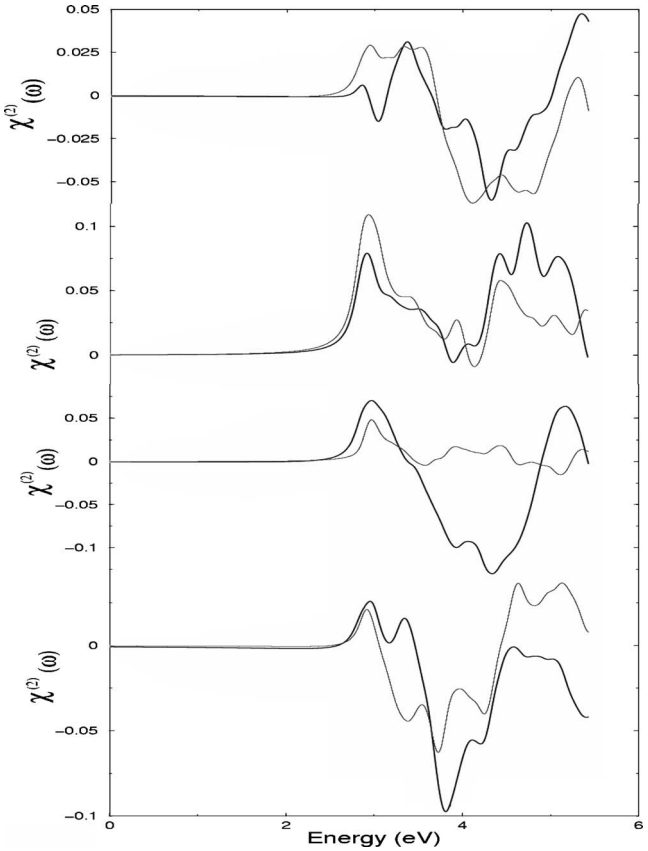

FIG. 6. (First panel) Calculated Im $\chi^{(2)}_{123}(\omega)$ (dark curve) and Im $\chi^{(2)}_{112}(\omega)$ (light curve). (Second panel) Calculated Im $\chi^{(2)}_{211}(\omega)$ (dark curve) and Im $\chi^{(2)}_{233}(\omega)$ (light curve). (Third panel) Calculated Im $\chi^{(2)}_{222}(\omega)$ (dark curve) and Im $\chi^{(2)}_{231}(\omega)$ (light curve). (Fourth panel) Calculated Im $\chi^{(2)}_{332}(\omega)$ (dark curve) and Im $\chi^{(2)}_{312}(\omega)$ (light curve). All Im $\chi^{(2)}(\omega)$ are multiply by 10^{-7}, in esu units.

LCB crystallizes in a noncentrosymmetric space group. This is the basic condition for a potential second harmonic generation material. According to the anionic group theory[25] the nonlinearity of a borate crystal originates from electrons formed by boron-oxygen group. So borates containing BO_3 groups or more complex groups formed by borate polyhedral such as B_3O_7, B_3O_8, and B_5O_{12} could be expected to possess a SHG effect 2–3 times larger than that of KDP. In fact, the LCB was found to have a Kurtz-Perry powder SHG effect about twice as large as that of KDP.[5] Normally in many materials several contributions to the nonlinear optical properties also give lattice vibrations (phonons in the crystals). But in borate materials the case is different due to relatively low longitudinal-optical-transfers-optical phonon infrared splitting contribution determined by ionicity of the particular chemical bonds.[26] Usually this contribution is more significant for the linear electrooptics effect[27] and for the SHG its contribution usually do not exceed 6–7% of the ionic part of the nonlinear optical susceptibility in the borate materials and particularly in these LCB borates is relatively slow (not higher than 7–8%) and may be neglected.

The calculated imaginary part of the SHG susceptibility $\chi^{(2)}_{abc}(\omega)$ for all eight components are shown in Fig. 6. A

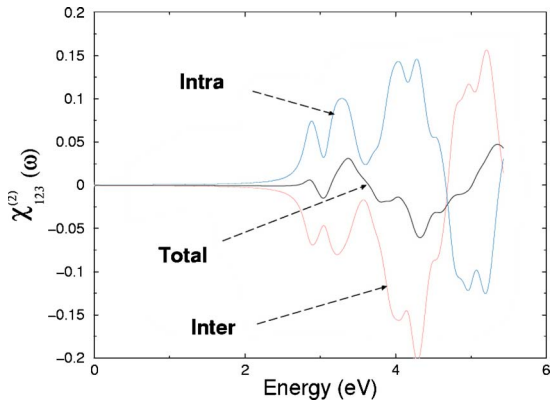

FIG. 7. (Color online) Calculated Im $\chi^{(2)}_{123}(\omega)$ along with the intraband (2ω) and interband (2ω) contributions. All Im $\chi^{(2)}(\omega)$ are multiply by 10^{-7}, in esu units.

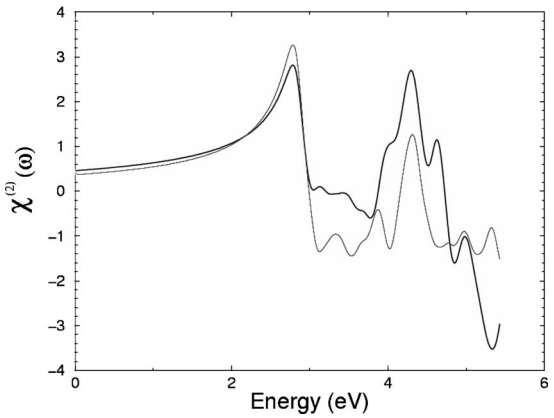

FIG. 8. Calculated Re $\chi^{(2)}_{211}(\omega)$ (dark curve) and Re $\chi^{(2)}_{233}(\omega)$ (light curve). Re $\chi^{(2)}_{211}(\omega)$ and Re $\chi^{(2)}_{233}(\omega)$ multiply by 10^{-12} pm/V, in SI units.

definite enhancement in the anisotropy on going from linear optical properties to the nonlinear optical properties is evident (Fig. 6). In Fig. 7, we show the 2ω interband and intraband contributions for the 123 component. We note the opposite signs of the two contributions throughout the frequency range. It is well known that nonlinear optical properties are more sensitive to small changes in the band structure than the linear optical properties. Hence any anisotropy in the linear optical properties is enhanced in the nonlinear spectra.

As can be seen the total SHG susceptibility is zero below half the energy band gap. The 2ω terms start contributing at energies $\sim 1/2E_g$ and the ω terms for energy values above E_g. In the low energy regime ($\leqslant$5 eV) the SHG optical spectra is dominated by the 2ω contributions. Beyond 5 eV the major contribution comes from the ω terms. The effective nonlinear coefficient d_{eff} is one of the most important parameters that characterizes the NLO properties of a crystal. The d_{eff} can be calculated using the second order nonlinear susceptibility d_{ij} of the crystal.[5,26] The effective nonlinear optical coefficient d_{eff} of LCB crystal estimated by comparison with other crystals[2] is 1.05 pm/V (at fundamental laser wavelength 1064 nm). We note that $\chi^{(2)}_{211}(\omega)$ is the dominant component (Fig. 8) which shows the largest total Re $\chi^{(2)}_{abc}(0)$ value compared to the other components (Table I).

The spectral features of Im $\chi^{(2)}_{abc}(\omega)$ can be understood from the dispersion of $\varepsilon_2(\omega)$. Unlike the linear optical spectra, the features for the SHG susceptibility are very difficult to identify from the band structure because of the presence of 2ω and ω terms. But we can make use of the linear optical spectra to identify the different resonance leading to various features in the SHG spectra. The structures in Im $\chi^{(2)}_{abc}(\omega)$ between 2.5–4.5 eV is mainly due to 2ω resonance. The structure from 4.5–5.5 eV is associated with interference between the ω fundamental resonance and double-frequency 2ω resonance. We present the values of $\chi^{(2)}_{abc}(0)$ for all the components in Table I.

IV. CONCLUSIONS

We have performed calculations of the energy band structure, DOS, frequency dependent linear and nonlinear optical response for LCB, using the FP-LAPW method. Our results for band structure and DOS show that LCB has an indirect energy band gap of about 4.45 eV. We have calculated $\varepsilon_2(\omega)$ and find a considerable anisotropy between $\varepsilon_2^{\perp}(\omega)$ and $\varepsilon_2^{\parallel}(\omega)$. Our calculations show that the birefringence of LCB possesses a positive sign, in agreement with the experimental data. The calculated SHG susceptibility shows that $\chi^{(2)}_{211}(\omega)$ is the dominant component. A definite enhancement in the anisotropy on going from linear optical properties to the nonlinear optical properties is evident.[28]

TABLE I. Calculated total and intraband and interband of the zero frequency of the real part of the Re $\chi^{(2)}_{abc}(\omega)$. The Re $\chi^{(2)}_{abc}(0)$ total, interband, and intraband are expressed in units of 1×10^{-7} esu. The total Re $\chi^{(2)}_{abc}(0)$ pm/V is expressed in 1×10^{-12} pm/V, in SI units.

Component	123	112	211	222	233	231	332	312
Re $\chi^{abc}(0)$*total*	−0.001	−0.005	0.011	0.01	0.01	0.0	−0.006	−0.002
Re $\chi^{abc}(0)$int *er*	−0.008	−0.01	−0.01	0.0	0.01	0.012	0.038	−0.004
Re $\chi^{abc}(0)$int *ra*	0.009	0.0025	0.015	0.012	0.005	−0.012	−0.048	−0.002
Total	−0.05	−0.15	0.55	−0.25	0.4	0.02	−0.25	−0.05
Re $\chi^{abc}(0)$pm/V								

ACKNOWLEDGMENTS

The authors would like to thank the Institute Computer Center, for providing the computational facilities. Also we thank Claudia Ambrosch-Draxl, 000 Montanuniversität Leoben, 8700 Leoben, Franz-Josef-StraBe 18, Austria, and Sangeeta Sharma, Institut für Theoretische Physik, Freie Universität Berlin, Arnimallee 14, D-14195 Berlin, Germany. This work was supported by the institutional research concept of the Institute of Physical Biology, UFB (Grant No. MSM6007665808) and the Institute of System Biology and Ecology, ASCR (Grant No. AVOZ60870520).

[1] C. Chen, Y. Wu, and R. Li, J. Cryst. Growth **99**, 790 (1990).
[2] G. Wang, J. Lu, D. Cui, Z. Xu, Y. Wu, P. Fu, X. Guan, and C. Chen, Opt. Commun. **209**, 481 (2002).
[3] Yicheng Wu, Peizhen Fu, F. Zheng, S. Wan, and X. Guan, Opt. Mater. **23**, 373 (2003).
[4] Y. C. Wu, P. Z. Fu, X. G. Guan, C. C. Chen, G. L. Wang, J. H. Lu, and Z. Y. Xu (unpublished).
[5] Y. Wu, J. Liu, P. Fu, J. Wang, H. Zhou, G. Wang, and C. Chen, Chem. Mater. **13** 753 (2001).
[6] Ali H. Reshak, S. Auluck, I. V. Kityk, A. Majchrowski, D. Kasprowicz, M. Drozdowski, J. Kisielewski, T. Lukasiewicz, and E. Michalski, J. Mater. Sci. **41**, 1927 (2006).
[7] Ali Hussain Reshak and S. Auluck, Physica B **358**, 158 (2005).
[8] Shiwu Gao, Comput. Phys. Commun. **153**, 190 (2003).
[9] Karlheinz Schwarz, J. Solid State Chem. **176**, 319 (2003).
[10] Y. Wu, J. Li, P. FuJ. Wang, F. Guo, G. Zhao, J. Qin, and C. Chen, Proc. SPIE **3556**, 8 (1998).
[11] P. Blaha, K. Schwarz, G. K. H. Madsen, D. Kvasnicka, and J. Luitz, WIEN2K, An augmented plane wave plus local orbitals program for calculating crystal properties, Vienna University of Technology, Austria, 2001.
[12] W. Kohn and L. J. Sham, Phys. Rev. **140**, A1133 (1965).
[13] M. S. Hybertsen and S. G. Louie, Phys. Rev. B **34**, 5390 (1986).
[14] T. Yamasaki, N. Suzuki, and K. Motizuki, J. Phys. C **20**, 395 (1987).
[15] Ali Hussain Reshak and S. Auluck, Phys. Rev. B **68**, 245113 (2003).
[16] Sangeeta Sharma, S. Auluck, and M. A. Khan, Pramana, J. Phys. **54**, 431 (1999).
[17] B. F. Levine, Phys. Rev. B **7**, 2600 (1973), and references therein.
[18] F. Nastos, B. Olejnik, K. Schwarz, and J. E. Sipe, Phys. Rev. B **72**, 045223 (2005).
[19] H. Tributsch, Z. Naturforsch. A **32A**, 972 (1977).
[20] F. Wooten, *Optical Properties of Solids* (Academic, New York, 1972).
[21] M. Iwai, T. Kobayashi, H. Furuya, Y. Mori, and T. Sasaki, Jpn. J. Appl. Phys., Part 1 **36**, 276 (2001).
[22] S. N. Rashkeev, W. R. L. Lambrecht, and B. Segall, Phys. Rev. B **57**, 3905 (1998).
[23] D. E. Aspnes, Phys. Rev. B **6**, 4648 (1972).
[24] W. Boyd, *Nonlinear Optics* (Academic Press, Boston, 1992).
[25] C. Chen, Y. Wu, and R. Li., Int. Rev. Phys. Chem. **8**, 65 (1989).
[26] I. V. Kityk, Sov. Phys. Solid State **33**, 1026 (1991).
[27] A. Mefleh, S. Benet, S. Brunet, H. Kaddouri, B. Sahraoui, I. V. Kityk, and M. Makowska Janusik, Opt. Mater. **13**, 339 (1999).
[28] R. L. Sutherland, *Handbook of Nonlinear Optics* (Marcel Dekker, New York, 1996), pp. 18, 36, 59.